Cell Metabolism
Article

The Combined Hyperlipidemia Caused by Impaired Wnt-LRP6 Signaling Is Reversed by Wnt3a Rescue

Gwang-woong Go,[1] Roshni Srivastava,[1] Antonio Hernandez-Ono,[2] Gyoungok Gang,[1] Stephen B. Smith,[3] Carmen J. Booth,[4] Henry N. Ginsberg,[2] and Arya Mani[1,5,*]
[1]Yale Cardiovascular Research Center, Department of Internal Medicine, Yale University School of Medicine, New Haven, CT 06511, USA
[2]Department of Medicine, Columbia University College of Physicians and Surgeons, New York, NY 10032, USA
[3]Department of Animal Science, Texas A&M University, College Station, TX 77843, USA
[4]Section of Comparative Medicine
[5]Department of Genetics
Yale University School of Medicine, New Haven, CT, 06520, USA
*Correspondence: arya.mani@yale.edu
http://dx.doi.org/10.1016/j.cmet.2013.11.023

SUMMARY

The underlying molecular genetic basis of combined hyperlipidemia, the most common atherogenic lipid disorder, is poorly characterized. Rare, nonconservative mutations in the Wnt coreceptor, LRP6, underlie autosomal dominant atherosclerosis, combined hyperlipidemia, and fatty liver disease. Mice with *LRP6*^{R611C} mutation similarly developed elevated plasma LDL and TG levels and fatty liver. Further investigation showed that *LRP6*^{R611C} mutation triggers hepatic de novo lipogenesis, lipid and cholesterol biosynthesis, and apoB secretion by an Sp1-dependent activation of IGF1, AKT, and both mTORC1 and mTORC2. These pathways were normalized after in vitro treatment of primary hepatocytes from *LRP6*^{R611C} mice with either the IGF1R antagonist PPP, rapamycin, or rmWnt3a. Strikingly, in vivo administration of rmWnt3a to *LRP6*^{R611C} mice normalized the altered expression of enzymes of DNL and cholesterol biosynthesis, and restored plasma TG and LDL levels to normal. These findings identify Wnt signaling as a regulator of plasma lipids and a target for treatment of hyperlipidemia.

INTRODUCTION

Familial combined hyperlipidemia (CHL), featuring elevated levels of plasma triglycerides (TGs) and low-density lipoprotein (LDL) cholesterol (C), is the most common form of hyperlipidemia found in the general population. Despite 40 years of investigation, no single gene has been clearly linked to this disorder, and its underlying molecular mechanisms remain poorly understood. We identified rare nonconservative loss of function mutations in the gene encoding Wnt coreceptor *LRP6* (OMIM, ADCAD2), which underlie autosomal dominant, early onset coronary artery disease (CAD), and metabolic syndrome traits, including elevated plasma TG and LDL-C levels, diabetes, osteoporosis, and hypertension (Mani et al., 2007; Singh et al., 2013b). These findings underscore the emerging evidence implicating effects of altered Wnt signaling on plasma lipids. Low serum levels of Wnt1 are associated with elevated TG and LDL-C in patients with premature CAD (Goliasch et al., 2012). Common genetic variants in genes encoding TCF7L2 are associated with elevated plasma TG in kindreds with familial combined hyperlipidemia (Delgado-Lista et al., 2011; Huertas-Vazquez et al., 2008), while genetic variants in LRP6 have been associated with risk for elevated LDL-C (Tomaszewski et al., 2009) in the general population. The functional characterization of the common genetic variants is hindered by their inherent small magnitude of effect on the trait. In contrast, the large effects imparted by the nonconservative *LRP6* mutations have allowed detailed studies of their effects both in vitro and in primary human cells. The studies of macrophages and skin fibroblasts of the *LRP6*^{R611C} mutation carriers have shown that elevated plasma LDL-C is, partially, the result of impaired receptor-mediated uptake of LDL (Liu et al., 2008; Ye et al., 2012). The contribution of LRP6 to LDL clearance was later confirmed by a genome-wide targeted RNAi screening of cholesterol-regulating genes (Bartz et al., 2009). LRP6 primarily facilitates LDL receptor (LDLR)-dependent LDL clearance in most human cells (Ye et al., 2012). LRP6 forms a complex with LDLR, clathrin, and autosomal recessive hypercholesterolemia protein and is required for clathrin-mediated vesicular LDL uptake (Ye et al., 2012). These functions are impaired in hematopoietic cells and skin fibroblasts of the *LRP6*^{R611C} mutation carriers, resulting in 15%–20% lower LDL clearance compared to wild-type (WT) cells. The same magnitude of reduction in LDL uptake occurs when LRP6 is knocked down by RNA interference. This modest reduction in LDL clearance, however, does not explain the severe degree of hyperlipidemia in *LRP6*^{R611C} mutation carriers, raising the possibility that increased synthesis and secretion of apolipoprotein B (apoB)-containing lipoproteins constitute major disease mechanisms. To address this question, we generated a mouse model of *LRP6*^{R611C} mutation (*Lrp6*$^{mut/+}$) by modifying the endogenous mouse *LRP6* through homologous recombination. To assess the LDLR-independent role of LRP6 in the hyperlipidemia present in this mouse, *Lrp6*$^{mut/mut}$ mice were crossbred onto

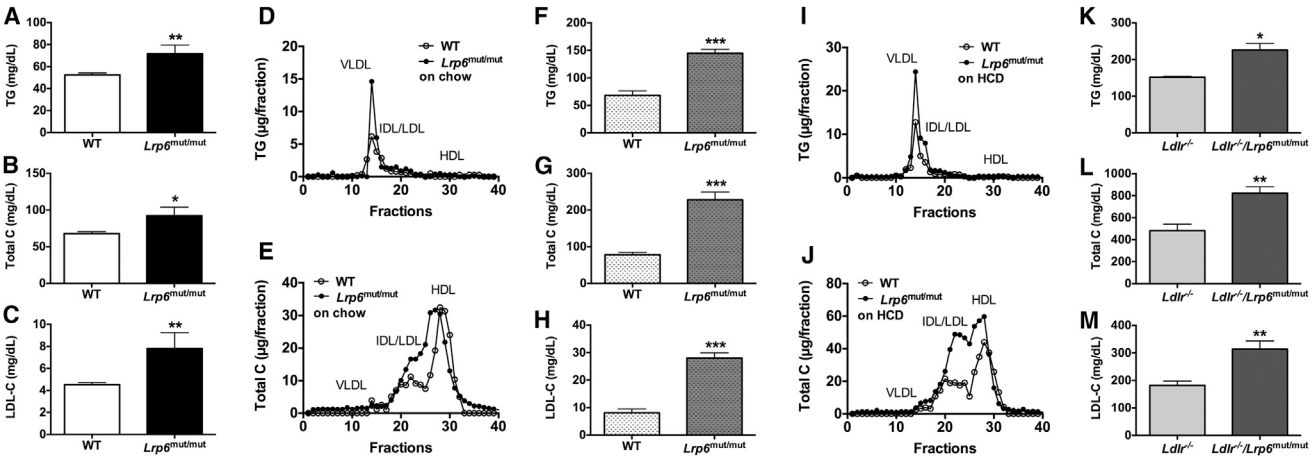

Figure 1. Plasma Lipid Profiles in *Lrp6*$^{mut/mut}$ and *Ldlr*$^{-/-}$/*Lrp6*$^{mut/mut}$ Mice

(A–C) Higher-plasma TG, total C, and LDL-C levels in *Lrp6*$^{mut/mut}$ mice on chow diet and (F–H) HCD compared to WT mice on same diets. (K–M) Higher-plasma TG, total C, and LDL-C levels in *Ldlr*$^{-/-}$/*Lrp6*$^{mut/mut}$ mice on HCD compared to *Ldlr*$^{-/-}$ mice on same diet. (D and E) Lipoprotein separation by FPLC in *Lrp6*$^{mut/mut}$ mice on chow diet and (I and J) HCD diet show higher TG content of VLDL and higher TC content of IDL/LDL in *Lrp6*$^{mut/mut}$ compared to WT mice. *$p < 0.05$; **$p < 0.01$; ***$p < 0.001$. WT, wild-type; HCD, high cholesterol diet; TG, triglycerides; Total C, total cholesterol; LDL-C, LDL cholesterol; FPLC, fast protein liquid chromatography. Error bars represent SD. See also Figure S1.

Ldlr$^{-/-}$ mice. The effect of *LRP6*^{R611C} mutation on plasma lipids and their regulation by Wnt/LRP6 pathways were examined in *Lrp6*$^{mut/mut}$ and *Ldlr*$^{-/-}$*Lrp6*$^{mut/mut}$ mice.

RESULTS

Lrp6$^{mut/mut}$ Mice Exhibit Elevated Plasma LDL-C and TG

Mice with *LRP6*^{R611C} (*Lrp6*$^{mut/+}$) on B57BL/6 background were generated by manipulating mouse endogenous *LRP6* through homologous recombination (see Experimental Procedures). Three-month-old heterozygote *Lrp6*$^{mut/+}$ mice on chow diet have significantly higher plasma TG, total C, and LDL-C compared to WT mice (see Figure S1 available online). These levels were intermediate between WT and homozygous mutants (Figure S1). Plasma lipids were significantly higher in homozygote *Lrp6*$^{mut/mut}$ mice compared to WT (Figures 1A–1C); homozygous mice were then used for further experimentation. There was no significant difference in free fatty acid levels between the two strains (data not shown). Lipid profiling of FPLC-separated lipoprotein fractions showed that, as expected, the increased TG in *Lrp6*$^{mut/mut}$ mice was predominantly associated with VLDL particles (Figure 1D). FPLC also showed higher non-HDL-C (IDL/LDL) in the mutant versus WT mice (Figure 1E). *Lrp6*$^{mut/mut}$ mice on 6 months of high-cholesterol/high-fat diet (HCD) (40% fat, 1.25% cholesterol, 0.5% cholic acid) had about 2-fold increase in plasma TG (Figure 1F) and about 3-fold increase in total C (Figure 1G) and LDL-C (Figure 1H) compared to WT littermates. FPLC-separated lipoprotein similarly showed higher TG in the VLDL fraction and higher cholesterol in the non-HDL-C fraction in *Lrp6*$^{mut/mut}$ versus WT mice on HCD (Figures 1I and 1J). We had previously shown that LRP6 regulates LDLR-mediated vesicular uptake of LDL. To examine the unique role of LRP6 in lipoprotein assembly and secretion, *Lrp6*$^{mut/mut}$ mice were crossbred onto *Ldlr*$^{-/-}$ mice to generate *Ldlr*$^{-/-}$/*Lrp6*$^{mut/mut}$ mice. Introducing the *LRP6*^{R611C} allele into *Ldlr*$^{-/-}$ mice background resulted in significant increase in plasma TG, total C, and LDL-C (Figures 1K–1M) in 9-month-old mice on HCD compared to *Ldlr*$^{-/-}$ mice. Since the effect of *LRP6*^{R611C} allele on LDL binding and clearance is relatively small (Liu et al., 2008; Ye et al., 2012) (Figures 2A and 2B), the major differences in plasma lipoproteins and lipids cannot be explained by decreased clearance and must be, therefore, the result of increased production of VLDL (see below).

Lrp6$^{mut/mut}$ Mice Develop Fatty Liver Disease

CHL is associated with nonalcoholic fatty liver disease (Angulo, 2002). Both 6-month-old WT and *Lrp6*$^{mut/mut}$ mice on HCD for 3 months developed fatty liver, but the fat content in *Lrp6*$^{mut/mut}$ mice was significantly higher (Figure 3A), which was associated with gross enlargement of the liver and elevated plasma levels of aspartate aminotransferase and bilirubin (Figures S2A and S2D). Accordingly, the neutral lipid storage assayed by Nile red staining was significantly greater in primary hepatocytes of *Lrp6*$^{mut/mut}$ versus WT mice on HCD (Figure 3B). Total hepatic TG and cholesterol ester (CE) contents were also significantly higher in *Lrp6*$^{mut/mut}$ versus WT mice (Figures 3C and 3D). No difference in β-oxidation was seen between primary hepatocytes from WT and *Lrp6*$^{mut/mut}$ mice (Figure 3E). The examination of fatty acid composition in the liver of *Lrp6*$^{mut/mut}$ mice showed greater 18:1n9 fatty acid content in *Lrp6*$^{mut/mut}$ compared to WT mice (Figure S3A). This finding was consistent with increased expression of SCD1, as will be shown. No difference was found in fatty acid contents of WAT between *Lrp6*$^{mut/mut}$ and WT mice (Figure S3B).

Increased TG/VLDL Synthesis and Secretion in *Lrp6*$^{mut/mut}$ Mice Are Associated with Enhanced Expression of Lipogenic Enzymes

We measured in vivo VLDL clearance in mice on chow diet by intravenous injection of ^{125}I-VLDL. The radioactivity remaining in apoB, the marker of VLDL particles, at 2, 30, 60, 120, and

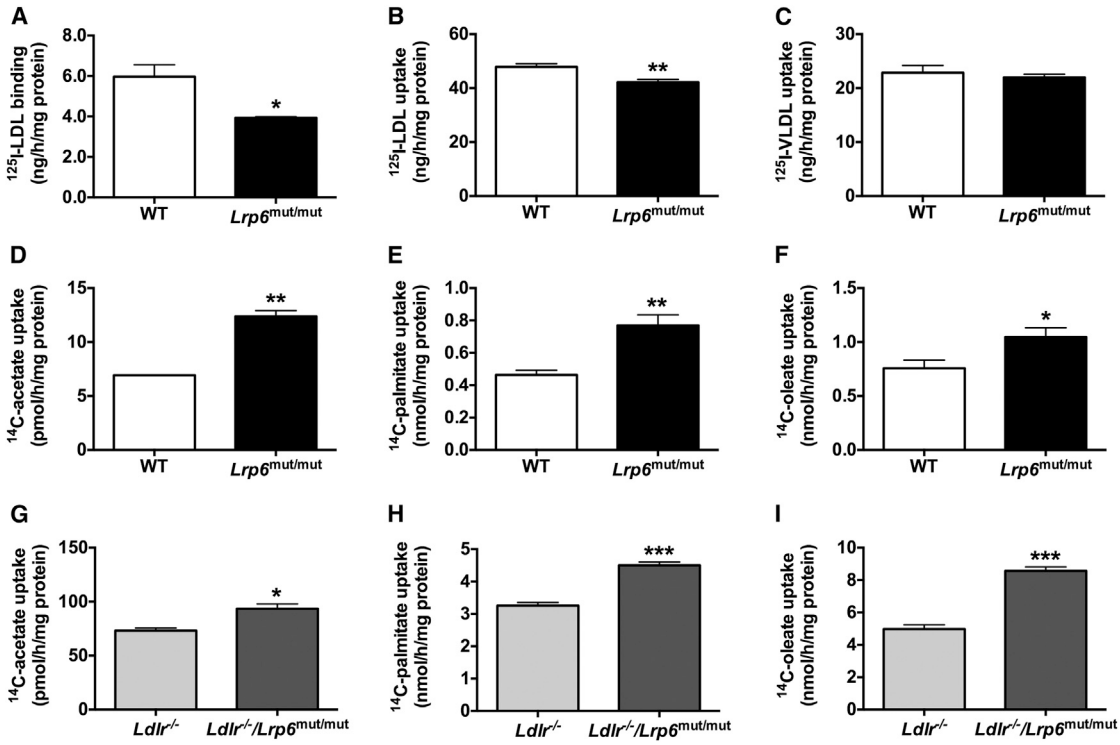

Figure 2. Binding and Uptake of Lipoproteins and Fatty Aicds in *Lrp6*$^{mut/mut}$ and *Ldlr*$^{-/-}$/*Lrp6*$^{mut/mut}$ Mice

(A) Binding and (B) uptake of ^{125}I-LDL and (C) uptake of ^{125}I-VLDL in *Lrp6*$^{mut/mut}$ and wild-type (WT) mice hepatocytes. (D) ^{14}C-acetate, (E) ^{14}C-palmitate, and (F) ^{14}C-oleate uptake by the hepatocytes of *Lrp6*$^{mut/mut}$ compared to WT mice. (G) Greater ^{14}C-acetate (H) palmitate and (I) oleate uptake by hepatocytes of *Ldlr*$^{-/-}$/*Lrp6*$^{mut/mut}$ compared to *Ldlr*$^{-/-}$ mice. *p < 0.05; **p < 0.01; ***p < 0.001. Error bars represent SD.

240 min after injection was used to determine clearance of VLDL in *Lrp6*$^{mut/mut}$ and WT mice. The experiment showed no differences in VLDL clearance between the two groups (Figure 4A). Similarly, there was no change in VLDL uptake by primary hepatocytes of *Ldlr*$^{-/-}$/*Lrp6*$^{mut/mut}$ versus *Ldlr*$^{-/-}$ mice (Figure 2C). To assess VLDL-apoB secretion, 6 hr fasted mice were injected i.p. ^{35}S-methionine and P407, a polyoxyethylene copolymer that blocks LPL-mediated lipolysis of VLDL in plasma. VLDL-apoB secretion, assayed by in vivo measurement of the appearance of newly secreted ^{35}S-methionine-labeled apoB100 radioactivity, was significantly greater in *Lrp6*$^{mut/mut}$ than in WT mice (Figure 4B). We next examined the TG secretion in 8- to 10-week-old *Lrp6*$^{mut/mut}$ and WT mice. Plasma TG levels rose immediately after i.p. P407 injection in both WT and *Lrp6*$^{mut/mut}$ mice but began to diverge after 1 hr and remained significantly higher at 24 hr in *Lrp6*$^{mut/mut}$ than in WT mice (Figure 4C). The combined apoB100 and TG results indicate significantly greater hepatic secretion of VLDL particles in *Lrp6*$^{mut/mut}$ compared to WT mice. To assess de novo lipogenesis (DNL) and TG synthesis, primary hepatocytes from *Lrp6*$^{mut/mut}$ and WT mice were incubated with ^{14}C-acetate, ^{14}C-plamitate, and ^{14}C-oleate. TG was isolated by thin-layer chromatography (TLC), and the ^{14}C incorporations were measured. The results showed 7-fold increase in incorporation of labeled acetate and greater than 60% increase of labeled palmitate and oleate into TG in *Lrp6*$^{mut/mut}$ mice compared to WT littermates (Figures 4D–4F). Similarly, there was increased incorporation of all three labels into TG in primary hepatocytes of *Ldlr*$^{-/-}$/*Lrp6*$^{mut/mut}$ mice compared to *Ldlr*$^{-/-}$ mice (Figures 4G–4I). Taken together, these findings indicated increased DNL and TG synthesis associated with increased VLDL secretion in HCD-fed mice with the *R611C* allele.

To explore the mechanisms that underlie enhanced DNL, TG synthesis, and VLDL secretion, mRNA and protein expression levels of MTP, apoB, and the key hepatic enzymes of DNL were compared between *Lrp6*$^{mut/mut}$ and WT mice on both chow diet and HCD. Protein and mRNA levels of ACC1, FASN, ELOVL6, SCD1, DGAT1, GPAT1, MTP, and apoB were all higher in *Lrp6*$^{mut/mut}$ liver than in WT littermates (Figures 4J and 4K; data shown for chow diet). These proteins are regulated by SREBP1 and LXRα (Basciano et al., 2009; Darimont et al., 2006; Wang et al., 2004). Accordingly, the expression levels of the mature form of SREBP1 and the level of LXRα in nuclear extracts were considerably higher in *Lrp6*$^{mut/mut}$ liver compared to WT littermates (Figure 4J). Similar changes were observed in mice with *Ldlr*$^{-/-}$ background (Figure S4). In concordance with this, ^{14}C-acetate, palmitate, and oleate uptake by *Lrp6*$^{mut/mut}$ mouse hepatocytes was significantly increased compared to WT mice (Figures 2D–2F). The same increase in uptake of these substrates was seen in hepatocytes from *Ldlr*$^{-/-}$/*Lrp6*$^{mut/mut}$ mice (Figures 2G–2I).

Lrp6$^{mut/mut}$ Allele Triggers Hepatic Cholesterol Biosynthesis

Ldlr$^{-/-}$/*Lrp6*$^{mut/mut}$ mice had significantly higher plasma LDL-C levels compared to *Ldlr*$^{-/-}$ mice. Since the effect of *LRP6*^{R611C}

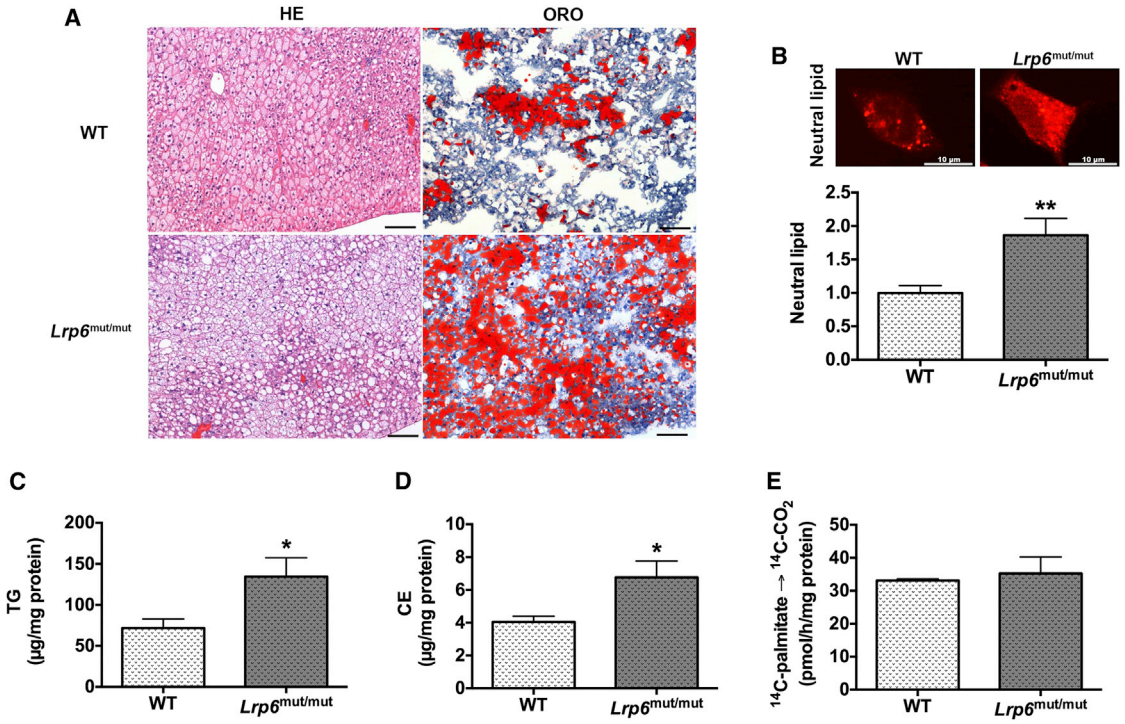

Figure 3. Fatty Liver in *Lrp6*$^{mut/mut}$ Mice

(A) Oil red O staining in 6-month-old mice on HCD shows greater amounts of hepatic fat in *Lrp6*$^{mut/mut}$ compared to WT mice. Scale bars, 100 μm. (B) Similarly, there is greater neutral lipid, assayed by Nile red staining, (C) and greater TG and (D) cholesterol ester (CE) content, measured by enzymatic assays in *Lrp6*$^{mut/mut}$ liver compared to WT mice. (E) No difference in fatty acid oxidation, assayed by ^{14}C-CO_2, was found between *Lrp6*$^{mut/mut}$ and WT mice. *$p < 0.05$; **$p < 0.01$. WT, wild-type; HCD, high-cholesterol diet; TG, triglycerides; CE, cholesterol ester. Error bars represent SD. See also Figures S2 and S3.

on LDL clearance is very small (Figures 2A and 2B), the difference could be exclusively explained by enhanced production of plasma LDL. Elevated LDL-C was from increased secretion of large VLDL particles (Figure S5). We compared hepatic C biosynthesis in primary hepatocytes of *Ldlr*$^{-/-}$/*Lrp6*$^{mut/mut}$ versus *Ldlr*$^{-/-}$ mice by measuring incorporation of ^{14}C-acetate and ^{14}C-oleate into free C (FC) and C ester (CE). ^{14}C incorporations into FC and CE were higher in mice *Ldlr*$^{-/-}$/*Lrp6*$^{mut/mut}$ versus *Ldlr*$^{-/-}$ mice (Figures 5A and 5B). These findings were consistent with increased hepatic mRNA and protein expression of HMGCR in *Ldlr*$^{-/-}$/*Lrp6*$^{mut/mut}$ versus *Ldlr*$^{-/-}$ mice (Figures 5C and 5D). In line with these results, the mature form of SREBP2, the key regulatory enzyme of C biosynthesis, was significantly higher in nuclear extracts from *Ldlr*$^{-/-}$/*Lrp6*$^{mut/mut}$ compared to *Ldlr*$^{-/-}$ mice (Figure 5D). SREBP1 and SREBP2 are retained in the ER by Insig1 and Insig2 (Yabe et al., 2002; Yang et al., 2002) and upon various conditions, including activation by AKT (Du et al., 2006), are transported with SCAP to Golgi for proteolytic cleavage (Hua et al., 1996) and subsequent translocation to nucleus. In line with increased expression of mature form of SREBPs and enhanced C biosynthesis, the expression levels of SCAP1 were increased and those of Insig1 and Insig2 were reduced in *Lrp6*$^{mut/mut}$ mice liver compared to WT littermates (Figure 5D). Genome-wide pattern of TCF7L2 chromatin occupancy has shown that TCF7L2 binds the 3′ transcription start site of Insig1 (Hatzis et al., 2008). Wnt is upstream of TCF7L2, and its impaired activity in *Lrp6*$^{mut/mut}$ is consistent with the diminished expression of Insig1 mRNA and protein. Higher hepatic expression levels of SCAP1 mRNA and protein in *Ldlr*$^{-/-}$/*Lrp6*$^{mut/mut}$ versus *Ldlr*$^{-/-}$ mice suggests inverse regulation of SCAP1 by Wnt/LRP6. This effect of LRP6 has not been previously described, and its underlying mechanisms are still unclear.

Activation of mTOR and IGF1 Pathways in *Lrp6*$^{mut/mut}$ Mice Liver

Plasma lipids levels in humans are influenced by nutrients. The nutrient-sensing kinase mTOR is the core component of multiprotein complexes mTORC1 and mTORC2, which regulate metabolism and lipid homeostasis by phosphorylating several ribosomal proteins, including S6, S6K, and 4E-BP1 (Laplante and Sabatini, 2009). mTORC1 is activated by PI3K/AKT and mTORC2 (Yecies et al., 2011), directly stimulates SREBP1 and SREBP2, and induces the expression of various lipogenic enzymes (Dalle Pezze et al., 2012; Hagiwara et al., 2012; Yuan et al., 2012). Phosphorylations of AKT (S473), S6K, S6, and 4E-BP1 were all significantly greater in *Lrp6*$^{mut/mut}$ mice liver compared to WT mice, both on chow diet (Figure 6A) and on HCD (data not shown).

In the liver, the PI3K/AKT pathway is primarily activated by insulin and IGF1 (Hagiwara et al., 2012). *Lrp6*$^{mut/mut}$ mice have normal baseline insulin and glucose levels but have an impaired response to intraperitoneal insulin administration (IPITT) (Figure 6B). Consistent with the plasma findings, dissection of insulin signaling revealed reduced tyrosine phosphorylation of IRS1 in

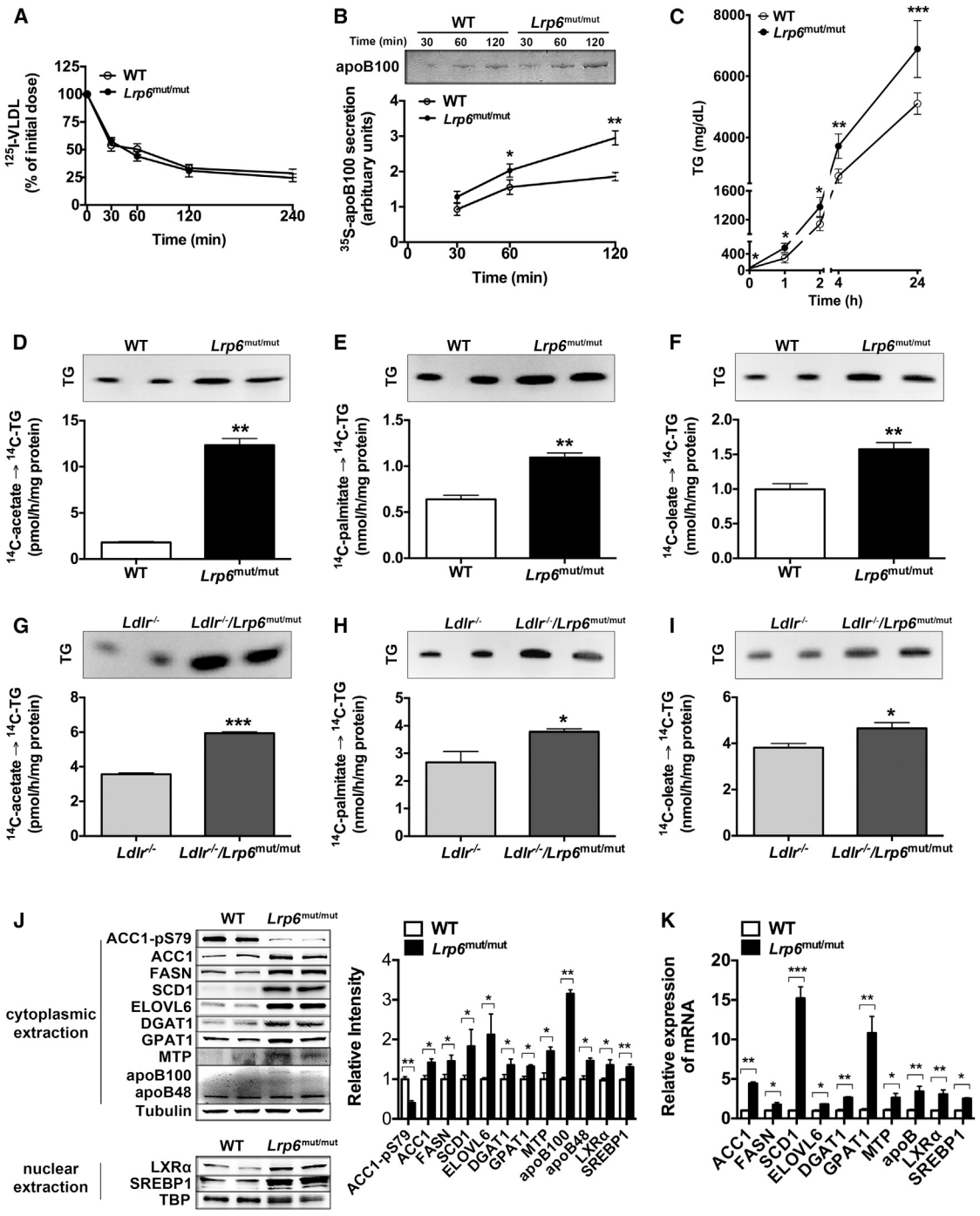

Figure 4. TG Synthesis and apoB Secretion

(A) Hepatic VLDL clearance was identical in *Lrp6*$^{mut/mut}$ and WT mice. (B) apoB secretion and (C) TG synthesis were higher in *Lrp6*$^{mut/mut}$ compared to WT mice. Incorporation of ^{14}C-acetate, ^{14}C-palmitate, and ^{14}C-oleate into TG by TLC were greater in (D–F) *Lrp6*$^{mut/mut}$ and (G–I) *Ldlr*$^{-/-}$/*Lrp6*$^{mut/mut}$ mice hepatocytes compared to WT and *Ldlr*$^{-/-}$ mice, respectively. (J) Protein and (K) mRNA expression of the hepatic enzymes of DNL, lipid synthesis and VLDL secretion and nuclear LXRα and SREBP1 were significantly higher in *Lrp6*$^{mut/mut}$ compared to WT mice. The relative intensities by densitometry are shown. *$p < 0.05$; **$p < 0.01$; ***$p < 0.001$. WT, wild-type; TG, triglycerides; VLDL, very low density lipoprotein; DNL, de novo lipogenesis; TLC, thin layer chromatography. Error bars represent SD. See also Figure S4.

Lrp6$^{mut/mut}$ mice liver compared to WT mice. However, AKT phosphorylation (S473) in response to insulin was paradoxically higher in *Lrp6*$^{mut/mut}$ compared to WT mice (same figure). This finding led to examination of IGF1/AKT pathway. Hepatic IGF1R protein and mRNA and plasma IGF1 protein were all expressed at significantly greater levels in *Lrp6*$^{mut/mut}$ compared

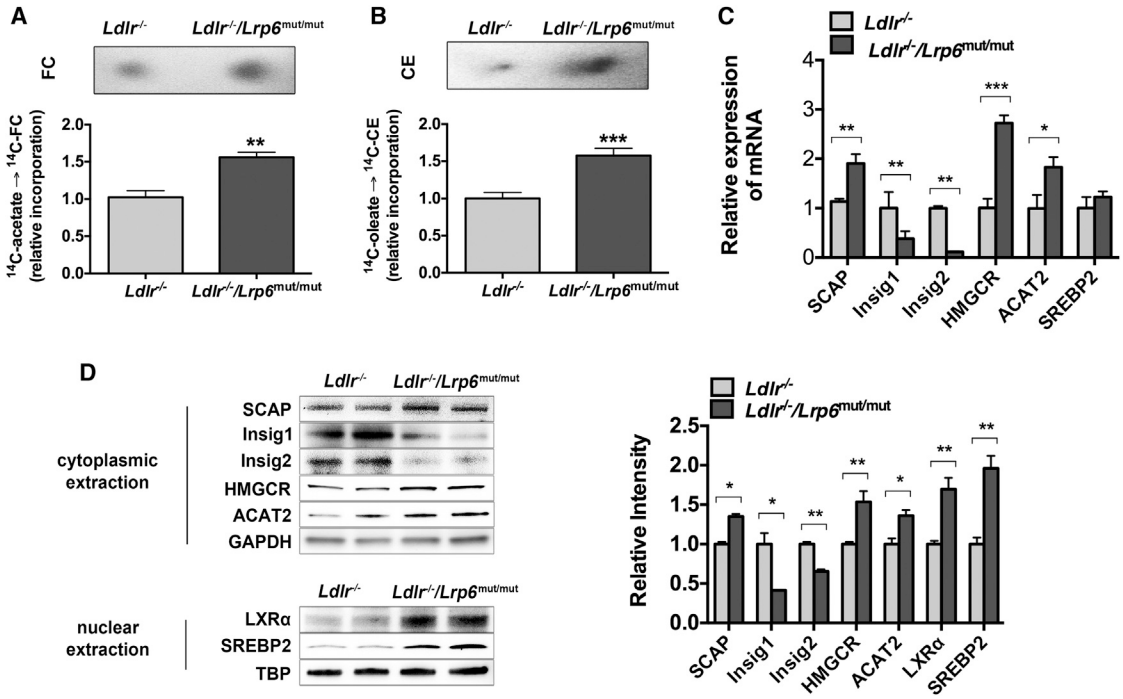

Figure 5. Cholesterol Biosynthesis in *Ldlr*$^{-/-}$ and *Ldlr*$^{-/-}$/*Lrp6*$^{mut/mut}$ Mice

Incorporation of (A) ^{14}C-acetate into FC and (B) ^{14}C-oleate into CE by TLC were much greater in primary hepatocytes from *Ldlr*$^{-/-}$/*Lrp6*$^{mut/mut}$ compared to *Ldlr*$^{-/-}$ mice. (C) mRNA and (D) protein expression levels of the key regulatory enzymes/proteins of cholesterol biosynthesis were significantly higher in *Ldlr*$^{-/-}$/*Lrp6*$^{mut/mut}$ compared to *Ldlr*$^{-/-}$ mice. The relative intensities by densitometry are shown. *p < 0.05; **p < 0.01; ***p < 0.001. FC, free cholesterol; CE, cholesterol ester; TLC, thin-layer chromatography. Error bars represent SD. See also Figure S5.

to WT mouse (Figures 6C–6E). IRS-1-independent AKT activation has been previously described in IRS-1-deficient mice (Araki et al., 1994). This finding suggests that impaired Wnt signaling (assayed by LRP6 and β-catenin phosphorylation, Figure 6C) enhances AKT phosphorylation despite hepatic insulin resistance, primarily through increased IGF1/IGF1R expression.

We have previously shown that IGF1R is ubiquitinated by LRP6 (Singh et al., 2013a). Impaired ubiquitination and increased sumoylation of IGF1R by *LRP6*^{R611C} result in increased IGF1R expression, which contributes to mTOR activation in response to insulin. LRP6 regulation of IGF1 was an important finding that required further exploration. Canonical Wnt upregulates Sp5, which suppresses the transcriptional activities of transcription factor Sp1 (Fujimura et al., 2007). IGF1 is transcriptionally regulated by Sp1 (Li et al., 2003; Zhu et al., 2000), hence its expression is likely diminished by Wnts activation. In contrast, the anticipation is that the *LRP6*^{R611C} mutation results in reduced Sp5 expression and enhanced Sp1-dependent transcription of IGF1. As predicted, the expression levels of Sp5 were markedly reduced in *Lrp6*$^{mut/mut}$ mice liver compared to WT mice (Figures 6C and 6D). The expression levels of Sp1 protein and mRNA were significantly higher in *Lrp6*$^{mut/mut}$ mice hepatocytes versus WT mice, but the relatively greater increase in protein level implied both transcriptional and posttranscriptional regulation by Wnt/LRP6 (same figure). We explored this possibility in HepG2 cells by sh-RNA-mediated knockdown of LRP6. LRP6 silencing led to reduced Sp5 and increased Sp1 protein (Figure 6F) and mRNA (Figure 6G) expressions, associated with increased expressions levels of lipogenic enzymes, SREBP1 and LXRα. Furthermore, lentiviral knockdown of Sp1 in primary mice hepatocytes resulted in significant decrease in protein levels of IGF1 and phosphorylation of AKT (AKT-pT308 and AKT-pS473) (Figure 6H). Consistent with these findings, treatment of primary mouse hepatocytes with the IGF1R inhibitor PPP abrogated AKT-dependent activation of mTOR pathway and reduced the expression of lipogenic enzymes (Figures S6A and S6B). These findings imply that the *LRP6*^{R611C} loss-of-function mutation increases hepatic IGF1 signaling and triggers the expression of lipogenic enzymes via the AKT/mTOR-dependent pathways.

Reduction of the Hepatic Lipogenic Enzymes with Rapamycin and Wnt3a Activation

The expression and activities of enzymes regulating DNL, TG synthesis, and C synthesis are dramatically reduced when primary mouse hepatocytes are treated either with the mTOR antagonist rapamycin (Figure 7A) or with recombinant mouse Wnt3a (rmWnt3a) (Figure 7B). Treatment with rmWnt3a for 72 hr was also associated with normalization of hepatocyte neutral lipid (Figure 7B). Given the positive response to in vitro rmWnt3a, we administered systemic rmWnt3a to *Lrp6*$^{mut/mut}$ mice (i.p. 25 μg/kg) every other day for 3 weeks. This resulted in the reduction of plasma TG (Figure 7C), total C (Figure 7D), and LDL-C (Figure 7E) in both WT and *Lrp6*$^{mut/mut}$ mice. These changes were associated with significantly reduced expression and/or activities of Sp1, IGF1, mTOR, ACC1, FASN, SCD1,

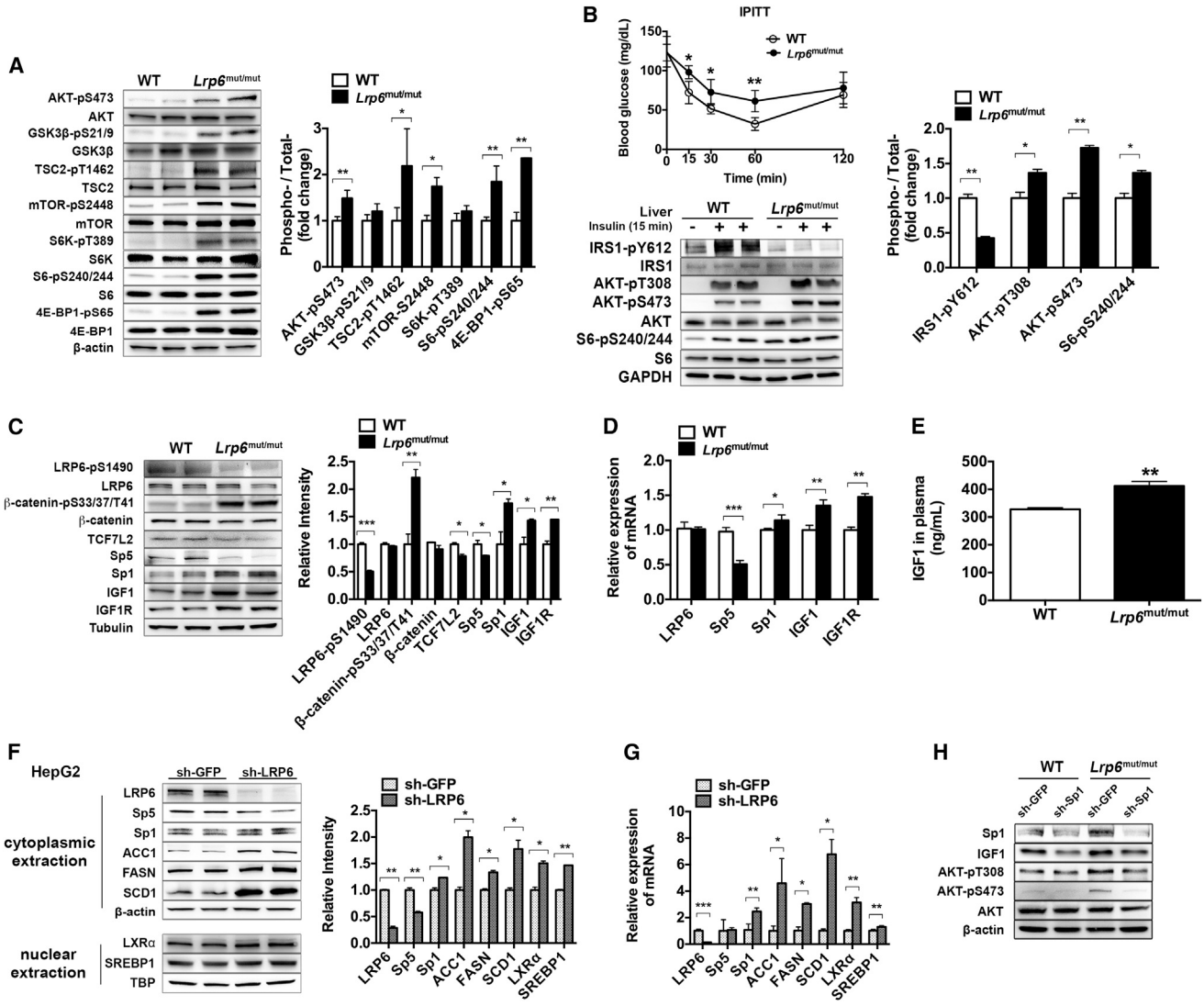

Figure 6. Activities of mTORC1, mTORC2, and IGF1 in *Lrp6*$^{mut/mut}$ Mice

(A) Western blot analysis demonstrating the greater activities of hepatic AKT/mTOR pathways in *Lrp6*$^{mut/mut}$ compared to WT mice. The ratios of phosphorylated to total proteins by densitometry are shown. (B) Intraperitoneal insulin tolerance test (IPITT) and hepatic insulin signaling pathway show impaired insulin signaling in *Lrp6*$^{mut/mut}$ compared to WT mice. The ratios of phosphorylated to total proteins by densitometry are shown. (C) Protein and (D) mRNA expression of the hepatic IGF1 and IGF1R, the transcription factors Sp1 and Sp5, and (E) plasma IGF1 were are higher in *Lrp6*$^{mut/mut}$ compared to WT mice. (F) Protein and (G) mRNA expression of transcription factors Sp5 and Sp1 and key enzymes of DNL are significantly altered after LRP6 silencing by shRNA in HepG2 cells. (H) Protein expression levels of Sp1, IGF1, and phosphorylation of AKT (pT308 and pS473) were significantly reduced by Sp1 knockdown in primary hepatocytes of WT and *Lrp6*$^{mut/mut}$ mice. *p < 0.05; **p < 0.01; ***p < 0.001. WT, wild-type; DNL, de novo lipogenesis. Error bars represent SD. See also Figure S6.

HMGCR, apoB, and MTP and reduced expression of the mature forms of SREBP1 and SREBP2 (Figure 7F). To examine whether rmWnt3a rescued the phenotype by signaling through the mutant LRP6, we stimulated primary hepatocytes of the mutant and WT mice with different doses of rmWnt3a. There was a shift to the right in the dose response to rmWnt3a in the mutant hepatocytes. However, higher doses of Wnt3a resulted in levels of phosphorylation of the mutant LRP6 that were similar to levels observed in WT receptor at lower doses (Figure S7). This increase in LRP6 phosphorylation was associated with significant reduction in expression of Sp1, IGF1, SREBP1, and SREBP2 (same figure). Taken together, these rescue studies implicate Wnt in regulation of mTOR/IGF1 pathways, DNL, lipid synthesis, and secretion of apoB/VLDL.

DISCUSSION

Altered Wnt signaling is an emerging risk factor for dyslipidemia by mechanisms that are not understood (Goliasch et al., 2012; Huertas-Vazquez et al., 2008; Perez-Martinez et al., 2012). We previously showed that Wnt coreceptor LRP6 regulates vesicular LDL uptake, a finding that was confirmed by subsequent studies (Bartz et al., 2009). Primary skin fibroblasts of *LRP6*^{R611C} mutation carriers exhibited 20% lower cellular LDL uptake compared

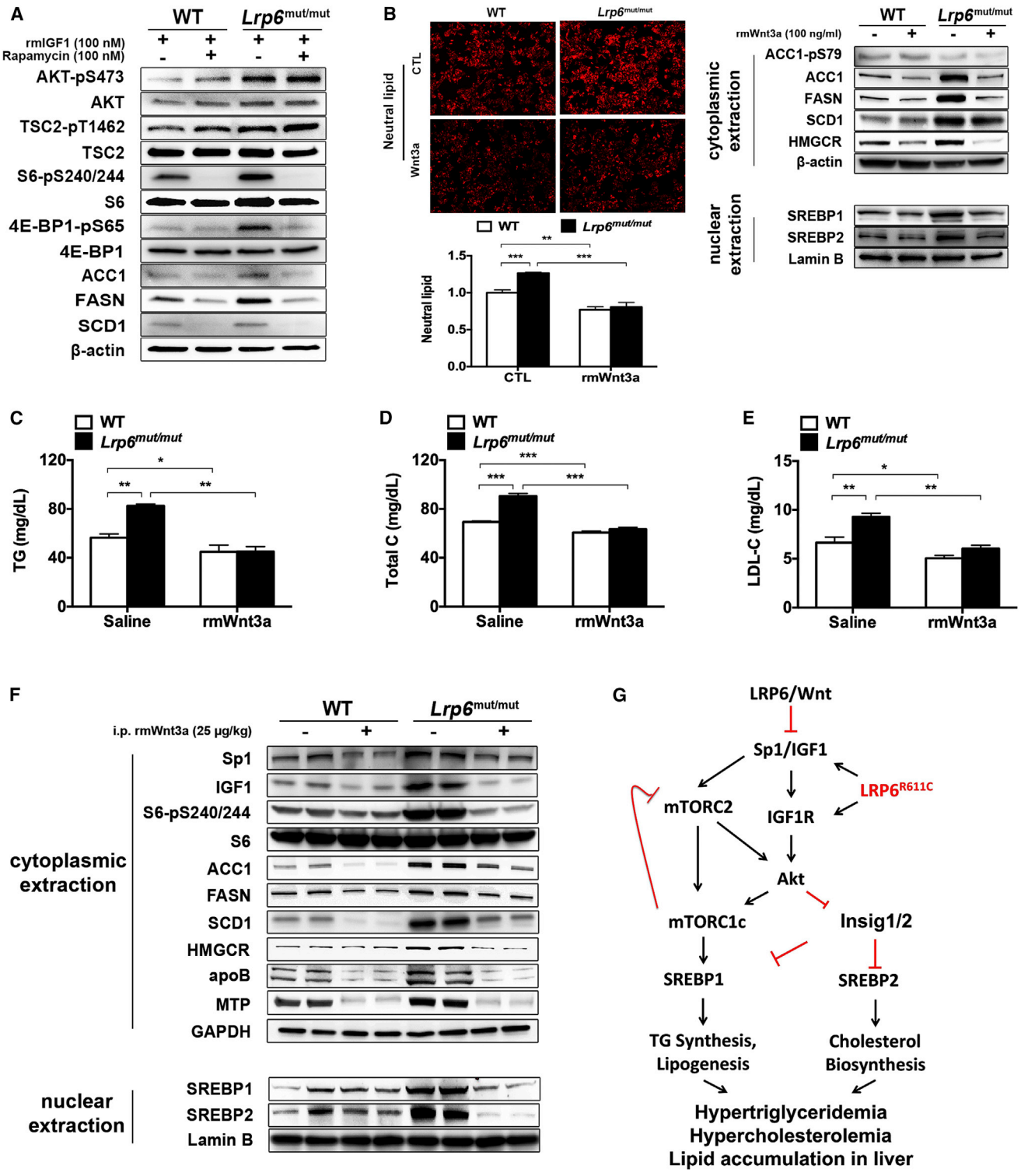

Figure 7. Normalization of Hepatic mTOR by Rapamycin and Reduction of Plasma Lipids by rmWnt3a in *Lrp6*$^{mut/mut}$ Mice

(A) mTOR inhibitor rapamycin reduced the activation of mTORC1 and the expression of enzymes of DNL in *Lrp6*$^{mut/mut}$ versus WT mice. (B) Normalization of hepatic neutral lipid, enzymes of DNL and C biosynthesis, and their regulators SREBP1 and SREBP2 by rmWnt3a in *Lrp6*$^{mut/mut}$ hepatocytes. (C) Normalization of plasma TG (D) total C (E) LDL-C and (F) enzymes of DNL and C biosynthesis after administration of i.p. rmWnt3a to *Lrp6*$^{mut/mut}$ mice. (G) The schematic of Wnt/LRP6 regulation of IGF1, IGF1R, mTOR pathways, DNL, TG synthesis, and C biosynthesis. *$p < 0.05$; **$p < 0.01$; ***$p < 0.001$. TG, triglycerides; C, cholesterol; rm, recombinant mouse; WT, wild-type; DNL, de novo lipogenesis. Error bars represent SD. See also Figure S7.

to fibroblasts from their unaffected relatives (Liu et al., 2008; Ye et al., 2012). The severity of hypercholesterolemia in *LRP6*^{R611C} mutation carriers could not, however, be explained by the modest degree reduction in LDL clearance; this prompted us to generate transgenic mice with *LRP6*^{R611C} mutation to examine its effect on hepatic lipid metabolism and VLDL synthesis and clearance. Here we show the important role of Wnt/LRP6 signaling in DNL, lipid synthesis, and apoB/VLDL secretion.

Lrp6$^{mut/mut}$ mice exhibited increased DNL, increased hepatic TG and C synthesis, and increased secretion of both VLDL apoB and TG compared to WT littermates. Higher hepatic DNL was associated with development of fatty liver in *Lrp6*$^{mut/mut}$ mice, a prominent feature of the metabolic syndrome (Angulo, 2002). These developments were coupled with increases in levels of mRNA and protein of enzymes of DNL, TG, and C synthesis, and their regulators SREBP1 and SREBP2, but not USF1, the transcription factor associated with FCHL (data not shown). AKT triggers SREBP1 and SREBP2 activation (Du et al., 2006) and suppresses Insig2a gene expression (Yecies et al., 2011), and there was increased hepatic AKT phosphorylation (S473), associated with enhanced activities of mTORC2 in *Lrp6*$^{mut/mut}$ mouse liver compared to WT mice. Further investigation revealed that increased hepatic IGF1 and IGF1R expression and action induce AKT/mTOR activation in *Lrp6*$^{mut/mut}$ mice. We had previously shown that LRP6 triggers IGF1R ubiquitination, while *LRP6*^{R611C} allele promotes its stabilization (Singh et al., 2013a). The effect of *LRP6*^{R611C} allele on IGF1 transcription was an important finding that we linked to impaired Wnt signaling. Earlier studies have shown that Sp1 is a transcriptional activator of IGF1 (Kaytor et al., 2001; Zhu et al., 2000). In this study we show that *Lrp6*$^{mut/mut}$ mouse hepatocytes have significantly greater Sp1 expressions compared to WT mice. shRNA-mediated silencing of LRP6 in primary hepatocytes increased Sp1 expression, further confirming the critical role of Wnt/LRP6 in regulation of this developmentally critical transcription factor. Taken together, these findings suggest that Wnt signaling tightly controls IGF1 expression and that its impaired function results in increased IGF1 and IGF1R expressions, leading to enhanced mTORC2/AKT activation as summarized in Figure 7G.

Consistent with earlier findings (Yecies et al., 2011), enhanced mTORC2-dependent AKT phosphorylation (S473) was associated with increased activation of mTORC1. The significance of mTORC1 pathway in regulation of DNL in *Lrp6*$^{mut/mut}$ mice was demonstrated by ex vivo treatment of *Lrp6*$^{mut/mut}$ liver cells with rapamycin, which significantly reduced the activity of mTORC1 and the expression of enzymes of DNL. As predicted, no change in activity of mTORC2, assessed by AKT S473 phosphorylation, was observed.

Finally, our most striking finding was the normalization of plasma LDL and TG by i.p. administration of rmWnt3a to *Lrp6*$^{mut/mut}$ mice, which were associated with reduced expression of mature forms of SREBP1 and SREBP2 and enzymes of DNL, TG, and C biosynthesis. In addition, Wnt3a treatment of *Lrp6*$^{mut/mut}$ mouse hepatocytes resulted in significant reduction of hepatic neutral lipid. These findings underscore the important role of Wnt signaling in homeostasis of plasma lipids and hepatic fat content and suggest that this pathway is a unique target for development of novel therapeutics against hyperlipidemia and FLD.

The rescue of hyperlipidemia trait with Wnt3a in a mouse with mutated LRP6 and impaired Wnt signaling is likely caused by improved interaction between ligand and its coreceptor. Study of crystal structure of LRP6 had suggested that R611C mutation impairs the salt bridge between R611 and E477 and weakens its ligand binding ability (Cheng et al., 2011). Earlier studies by our group (Mani et al., 2007) and others have shown that impaired Wnt signaling caused by R611C mutation can be rescued by higher doses of Wnt3a or by application of recombinant biglycan, an extracellular matrix protein that facilitates formation of a complex between Wnt3a and LRP6 (Berendsen et al., 2011). In the current study we show a shift to right in the dose response to rmWnt3a in mutant hepatocytes. Strikingly, higher-dose rmWnt3a normalized phosphorylation of the mutant LRP6 and was associated with significant reduction in expression of Sp1, IGF1, SREBP1, and SREBP2.

In summary, our study establishes a causal link between *LRP6* mutation/altered Wnt signaling and combined hyperlipidemia and elucidates the mechanisms by which Wnt signaling regulates lipogenesis, lipid synthesis, and apoB secretion. Rescue of the hyperlipidemia trait by Wnt3a in mice identifies the Wnt signaling pathway as a potential target for development of novel therapeutics against combined hyperlipidemia.

EXPERIMENTAL PROCEDURES

Generation of *LRP6*^{R611C} Mice

Mice with *LRP6*^{R611C} (*Lrp6*$^{mut/+}$) mutation on B57BL/6 background were generated by manipulating mouse endogenous *LRP6* through homologous recombination. Briefly, constructs containing mouse homologous DNA with two nucleotide mutations at the positions 100443-5, which results in R593C (mouse equivalent of human *R611C* mutation) substitution were generated by the Vegalab LLC (Wilmington, DE). C57BL/6 ESCs were injected with the constructs and targeted into the Balb/c blasts to generate chimeras. Chimeras were crossed with B6 mice, and genotype-positive mice were backcrossed for eight generations prior to experimentation. Three-month-old heterozygous *Lrp6*$^{mut/+}$ mice had modest elevation of plasma TG. *Lrp6*$^{mut/+}$ mice were intercrossed to obtain homozygous offspring in the expected Mendelian ratios. The viable offspring were genotyped by PCR (for primers, see Table S1). Homozygote (*Lrp6*$^{mut/mut}$) mice showed normal reproductive activities and had normal size and growth. Southern blot analysis of a limited number of mice confirmed the presence of *LRP6*^{R611C} allele only (data not shown). The mutant LRP6 protein was expressed in most tissues, including liver, skeletal muscle, and adipose tissue at normal levels. Homozygote *Lrp6*$^{mut/mut}$ were crossbred onto *Ldlr*$^{-/-}$ mice. The F1 progenies (*Ldlr*$^{-/+}$/*Lrp6*$^{mut/+}$) were backcrossed with *Ldlr*$^{-/-}$ mice to obtain offspring that were heterozygous for the R611C allele and LDLR deficient (*Ldlr*$^{-/-}$/*Lrp6*$^{mut/+}$). Subsequent intercross of these mice resulted in offspring that were homozygote for R611C allele and were LDLR deficient in the expected Mendelian ratios.

Mice were fed ad libitum and at age 6–8 weeks were fed with either a normal chow diet (9% kcal from fat) or a HCD for 3 months (40% kcal from fat, 1.25% cholesterol, 0.5% cholic acid; Research Diet, D12109). Experiments were carried out after overnight fasting. Each experiment was carried out in six to seven mice. After mice were sacrificed, tissues were snap frozen and plasma was separated, followed by storage at −80°C for further analysis. All procedures were approved by the Institutional Animal Care and Use Committee at Yale University.

Antibodies

Antibodies to ACC1-pS79, ACC1, FASN, SCD1, tubulin, TBP, GAPDH, AKT-pS473, AKT, GSK3β-pS21/9, GSK3β, TSC2-pT1462, TSC2, mTOR-pS2448, mTOR, S6K-pT389, S6K, S6-pS240/244, S6, 4E-BP1-pS65, 4E-BP1, β-actin, LRP6-pS1490, LRP6, TCF7L2, β-catenin, β-catenin-pS33/37/T41, IGF1R, AKT-pT308, and Lamin B were purchased from Cell Signaling. Antibodies to

apoB, SCAP, Insig1, Insig2, Sp5, and Sp1 were purchased from Santa Cruz Biotech. Antibodies to MTP, SREBP1, SREBP2, and IRS1 were purchased from BD Biosciences. Antibodies to ACAT2 and IGF1 were purchased from Novus. Antibodies to ELOVL6 (Thermo Scientific), DGAT1 (Bio Vision), GPAT1 (GeneTex), LXRα (Abcam), HMGCR (Upstate), and IRS1-pY612 (Invitrogen) were used for western blotting.

Primary Hepatocyte Isolations

Primary hepatocytes were isolated by perfusing portal vein of 3-month-old WT and *Lrp6*$^{mut/mut}$ male mice and 6-month-old *Ldlr*$^{-/-}$ mice and *Ldlr*$^{-/-}$/*Lrp6*$^{mut/mut}$ male mice on indicated diets (n = 6) with collagenase (type II collagenase, GIBCO). Isolated hepatocytes were Percoll purified and cultured on collagen-coated tissue culture dishes in William's medium supplemented with primary hepatocytes maintenance supplements (GIBCO) and kept in a humidified cell culture incubator at 37°C and 5% CO_2.

Generation of Stable LRP6 or Sp1 Knockdown Cells

For LRP6 knockdown in HepG2 cells, cells were maintained in Dulbecco's modified Eagle's medium (DMEM) containing 10% heat-inactivated fetal bovine plasma and 1× penicillin-streptomycin at 37°C in a humidified O_2/CO_2 (19:1) atmosphere. Lentivirus particles containing LRP6 targeting shRNA (5′-CGGCGAATTGAAAGCAGTGAT-3′) were purchased (Santa Cruz Biotech) and transduced into HepG2 cells. Transduced cells were selected using 1 μg/mL puromycin.

For Sp1 knockdown, isolated primary hepatocytes were cultured on collagen-coated tissue culture dishes in William's medium supplemented with primary hepatocytes maintenance supplements (GIBCO). Cells were infected with Sp1 shRNA (m) lentiviral Particles (sc-29488-V, Santa Cruz Biotech) using polybrene to increase the efficiency of infection.

Plasma and Liver Lipid Determination

Blood from fasted animals was obtained, and plasma was separated (1,500 g for 15 min). Plasma TG, total C, and LDL C were analyzed at the Mouse Metabolic Phenotyping Center at Yale by COBAS Mira Plus (Roche). Liver tissues were homogenized in 5% NP-40 in water slowly heated to 95°C for 5 min. Collected supernatants after centrifugation (14,000 g for 10 min) were assayed for total hepatic C and TG content using colorimetric enzymatic kit (Wako).

Lipoprotein Profiling by Fast Protein Liquid Chromatography

Plasma lipoprotein profiling was determined by fast protein liquid chromatography (FPLC). In brief, plasma from ten mice from each genetic background was pooled for FPLC analysis. A total of 200 μl plasma was loaded and run on the system followed by fractionation. Cholesterol levels of the fractions containing the plasma lipoproteins were analyzed by standard enzymatic assays using lipoprotein diagnostic kits (Wako).

Measurement of Hepatic Lipogenesis

Isolated primary hepatocytes of WT, *Lrp6*$^{mut/mut}$, *Ldlr*$^{-/-}$, and *Ldlr*$^{-/-}$/*Lrp6*$^{mut/mut}$ mice were serum starved overnight, followed by insulin stimulation (100 nM) for 4 hr. Insulin stimulated primary hepatocytes were incubated with 25.0 nmol of [1,2-^{14}C]-acetate (PerkinElmer), 12.5 nmol [1-^{14}C]-plamitate (PerkinElmer), and 12.5 nmol [1-^{14}C]-oleate (PerkinElmer) for 2 hr. Cells were washed three times with PBS before harvest in Cellstripper (Cellgro). Total lipid from cells was prepared by the Bligh and Dyer method (Bligh and Dyer, 1959). Concentrated neutral lipids were dissolved in chloroform: methanol (2:1, v/v) and lipid fractions were separated by TLC (Silica 60 F_{254}, Merck) using the organic mobile solvents hexane/diethylether/acetic acid (70:30:1 v/v). Lipids dots were visualized under UV light, and radioactivity was determined using a scintillation counter and normalized to protein concentrations.

Clearance of ^{125}I-VLDL Particles

The rate of VLDL particle clearance from plasma was determined using ^{125}I-labeled VLDL (Biomedical Technologies, Inc.). In brief, 3-month-old chow-diet-fed WT and *Lrp6*$^{mut/mut}$ mice were fasted for 4 hr at the beginning of light cycle to remove chylomicron. Mice were injected with 200 μl i.v. bolus of ^{125}I-VLDL (15 μg in 10 mM TrisCl [pH 7.4], 150 mM NaCl, and 0.2% [w/v] BSA). Blood collection was performed at 2 (baseline), 30, 60, 120, and 240 min, and plasma was separated immediately. To separate VLDL fraction from plasma, plasma in 750 μl KBr solution (d = 1.006 g/mL) was placed in an ultracentrifuge (Thermo Scientific, NC) and spun at 90,000 rpm for 3 hr at 4°C. The radioactivity of ^{125}I-labeled VLDL in plasma at each time point was determined by gamma counter after isopropanol precipitation of apoB. The remaining amount of ^{125}I-VLDL apoB was calculated as a percentage of the initial concentration 2 min after injection.

Measurement of apoB Secretion In Vivo

The accumulation of ^{35}S-methionine-labeled apoB in plasma was used to determine VLDL production rate. Briefly, 3-month-old chow-diet-fed WT and *Lrp6*$^{mut/mut}$ mice were fasted for 6 hr. The mice were anesthetized with 30% isoflurane in propylene glycol, followed by i.p. injection of 200 μl bolus containing 200 μCi ^{35}S-methionine and 1,000 mg/kg i.p. Poloxamer-407 (P407, BASF), an inhibitor of lipoprotein lipase in sterile PBS. Blood samples were collected at 30, 60, and 120 min after injection. Total protein synthesis after injection was calculated by measuring radioactivity of TCA precipitable protein in plasma. Adjusted volumes of plasma in sample buffer were applied to SDS-PAGE gel and visualized by Coomassie blue staining (SimplyBlue, Invitrogen) and scanned for densitometry.

TG Synthesis Using P407 Injection

To measure hepatic TG production, mice were injected with P407 at 1,000 mg/kg BW after 4 hr fasting. Plasma samples were collected at 0, 1, 2, 6, and 24 hr following injection. TG in plasma at each time point was measured using an enzymatic kit (Wako). The TG production rates were calculated from the differences in plasma TG levels over a given interval following detergent injection.

Cholesterol and Cholesterol Ester Biosynthesis In Vitro

The cholesterol synthesis was determined by measuring the incorporation of [1,2-^{14}C]-acetate into cellular sterol. Isolated primary hepatocytes of *Ldlr*$^{-/-}$ and *Ldlr*$^{-/-}$/*Lrp6*$^{mut/mut}$ mice were incubated with 25.0 nmol of [1,2-^{14}C]-acetate for 72 hr at 37°C. [1,2-^{3}H]-cholesterol was added to the aliquots as an internal standard (0.04 μCi/sample), and the solutions were saponified using KOH in 100% ethanol (60°C for 1 hr). Concentrated lipid aliquot resolved in small volume of dichlromethane was applied to TLC (Silica gel 60, EMD), using petroleum ether/diethyl ether/acetic acid (70:30:1). Cholesterol dots were visualized with 1% ferric (III) chloride in 50% aqueous ethanol and were scraped off for radioactivity determination.

Cholesterol ester synthesis was determined by incubating primary hepatocytes with [1-^{14}C]-oleate for 4 hr, using same steps as described above. Neutral lipid collection and TLC separation were performed as described above. Cholesterol ester fractions were scraped off, and the radioactivity was determined. Each condition was assayed in quadruples and normalized to internal standard and protein concentrations in the original lysates.

In Vitro Assessment of β-Oxidation

The β-oxidation was assessed by trapping radioactive CO_2 as described elsewhere (Krieg et al., 2004). Briefly, isolated primary hepatocytes from 3-month-old WT and *Lrp6*$^{mut/mut}$ mice were incubated in vitro with 0.5 μCi [1-^{14}C]-palmitic acid in William's medium for 2 hr. Culture flasks were tightly attached to customized CO_2 capture devices (Adams and Chittenden Scientific Glass). At the end of the 2 hr incubation period, reactions were rapidly terminated by addition of 5 N H_2SO_4, and cells were incubated for additional 30 min to complete CO_2 effervescence from the culture medium. The radioactivity of the filter paper was determined.

Nile Red Staining

Isolated primary hepatocytes were cultured on collagen-coated glass coverslips. Cells were fixed with 4% paraformaldehyde in PBS and stained with 0.1 μg/mL Nile red for 30 min. Specimens were examined by Nikon Ti-E Eclipse inverted microscope using excitation emission filters at 488 and 561 nm, respectively. Images were acquired at same setting of laser output, gain, and offset for three independent experiment, and 20 cells were randomly selected and analyzed from each coverslip. Similar experiment was carried out after primary hepatocytes were treated with rmWnt3a for 72 hr.

Fatty Acids Composition by Gas Chromatography

Lipid was extracted from liver tissues by the Folch method (Folch et al., 1957), and fatty acids were saponified by KOH and methylated with boron fluoride-methanol (BF_3) in methanol (Morrison and Smith, 1964). Fatty acid methyl esters were analyzed by gas chromatography (Varian model CP-3800 equipped with a CP-8200 autosampler, Varian Inc.). Separation of fatty acid methyl esters was accomplished on a fused silica capillary column (100 m 9 0.25 mm ID) (model CP-7420, Varian Inc.). An authentic standard (GLC 68-D, Nu-Chek Prep) was used to identify each peak.

Immunoblotting

Cytoplasmic and nuclear proteins were prepared using NE-PER nuclear and cytoplasmic extraction kit (Thermo Scientific, #78833). Cell lysates were processed and applied to SDS-PAGE and were immunoblotted using target primary antibodies followed by appropriate HRP-conjugated secondary antibodies. Enhanced chemiluminescence reagents were applied to develop the blots, and blots were quantified with Bio-Rad Image Lab.

Quantitative RT-PCR

Total RNA was isolated from cultured cells using RNeasy Plus Mini Kit (QIAGEN), and complementary DNA was synthesized from 5 μg of total RNA primed with random hexamer and using Superscripts II reverse transcriptase. Real-time PCR amplification was performed using specific primers (Tables S2 and S3) and iQ SYBR Green Supermix (Bio-Rad). Reactions were performed in quadruple with an 18S internal control. Relative quantification of mRNA levels was expressed as fold increase relative to the control.

Intraperitoneal Insulin Tolerance Tests

Mice were fasted for 6 hr and i.p. injected with 0.75 U/kg insulin (Sigma). Blood glucose and insulin levels were monitored from tail veins at 0, 15, 30, 45, 60, and 120 min using a glucometer (OneTouch Ultra2, LifeScan). For the insulin signaling experiment, mice were fasted for 6 hr and i.p. injected with 0.75 U/kg insulin. After 20 min, mice were sacrificed and tissues were snap frozen for further analysis of immunoblotting.

Analysis of Liver Function and Histology

Six-month-old WT and $Lrp6^{mut/mut}$ mice fed HCD for 3 months were sacrificed for microscopic analysis of lipid content and in vivo function test. Plasma was prepared for biochemical analysis. Aspartate aminotransferase, alanine aminotransferase, total bilirubin, albumin, and total protein were measured by 7600-020 clinical analyzer (Hitachi). Liver tissues were embedded in Tissue-Tek OCT cryostat molds (Leica) and frozen at −80°C. These tissues were used to generate 10-mm-thick sections in a cryostat. Tissue sections were stained in 0.5% oil red O and counterstained with Mayer's hematoxylin or with hematoxylin and eosin for gross histological examinations.

Rapamycin, IGF1, and Wnta3a Treatment In Vitro

Isolated primary hepatocytes were cultured with 100 nM rapamycin for 12 hr and stimulated with 1 μg/mL recombinant mouse IGF1 for 15 min. Whole-cell lysates were analyzed by immunoblotting for the measurement of total and phosphorylated proteins. For Wnt3a treatment, isolated primary hepatocytes were treated with 100 ng/mL recombinant mouse Wnt3a (rmWnt3a, R&D Systems) for 12 hr, and the lysates were immunoblotted to examine protein and phosphoprotein expressions.

Intraperitoneal rmWnt3a Administration

Mice were injected with i.p. with 25 μg/kg rmWnt3a every other day for 3 weeks. Mice were sacrificed, and plasma was collected for lipid profiling as described. Liver tissues were harvested for immunoblotting.

In Vitro Measurement of Fatty Acids Uptake

Isolated primary hepatocytes of WT, $Lrp6^{mut/mut}$, $Ldlr^{-/-}$, and $Ldlr^{-/-}/Lrp6^{mut/mut}$ mice were serum starved overnight, followed by insulin stimulation (100 nM) for 4 hr. Insulin-stimulated primary hepatocytes were incubated with 25.0 nmol of [1,2-^{14}C]-acetate, 12.5 nmol [1-^{14}C]-palmitate, and 12.5 nmol [1-^{14}C]-oleate for 30 min. Uptake was terminated using ice-cold PBS supplemented with 2% BSA. Whole lysate was subjected to radioactivity counting. Each condition was assayed in quadruples, and protein concentration of parallel cultures was measured using Bradford assay.

In Vitro Uptake of LDL and VLDL

Isolated primary hepatocytes of WT and $Lrp6^{mut/mut}$ mice were serum starved overnight, followed by treatment with ^{125}I-LDL or ^{125}I-VLDL (Biomedical Technologies, Inc.). For binding assays, cells were prechilled at 4°C followed by adding 10 μg/mL ^{125}I-LDL in DMEM supplemented with lipoprotein-deficient serum for 2 hr at 4°C. Cells were incubated with 2 ml of sodium dextran sulfate (4 mg/mL, Sigma). An aliquot was placed in gamma counter to determine the total amount of ^{125}I-LDL bound to the cell surface. Cells were harvested, and the lysate was used to measure protein concentration. For LDL or VLDL uptake, cells were incubated in lipoprotein-deficient serum with 10 μg/mL ^{125}I-LDL or ^{125}I-VLDL for 2 hr at 37°C. Harvested cell lysate was applied for radioactivity determination as described previously.

$VLDL_1$ and $VLDL_2$ Separation

Large VLDL ($VLDL_1$; S(f) = 60–400) and small VLDL ($VLDL_2$; S(f) = 20–60) were separated by ultracentrifugation density gradient technique after Lindgren, Jensen, and Hatch as described previously (Al-Shayji et al., 2007). TG concentration was then measured in each component with colorimetric enzymatic kit (Wako).

IGF1 and IGF1R Inhibitor

Primary mice hepatocytes were cultured on collagen-coated tissue culture dishes in William's medium supplemented with primary hepatocytes maintenance supplements (GIBCO). Cells were serum starved overnight before the addition of 1 μM picropodophylin (PPP, Calbiochem) for 24 hr or/and 100 nM recombinant human IGF1 (R&D Systems) for 15 min or 24 hr. Whole-cell lysates were analyzed by immunoblotting as described previously.

Statistical Analysis

All mice studies included seven mice in each group and were repeated at least twice. All in vitro studies were carried out in quadruple. Comparisons between two groups were performed using Student's t test. For multiple comparisons, LSD test in conjunction with ANOVA was carried out. Data are mean ± SD, and statistical significance is defined as $p < 0.05$.

SUPPLEMENTAL INFORMATION

Supplemental Information includes seven figures and three tables and can be found with this article at http://dx.doi.org/10.1016/j.cmet.2013.11.023.

ACKNOWLEDGMENTS

This study was supported by National Institutes of Health grant R01HL094784-05 (to A.M.).

Received: July 14, 2013
Revised: October 25, 2013
Accepted: November 30, 2013
Published: February 4, 2014

REFERENCES

Al-Shayji, I.A., Gill, J.M., Cooney, J., Siddiqui, S., and Caslake, M.J. (2007). Development of a novel method to determine very low density lipoprotein kinetics. J. Lipid Res. *48*, 2086–2095.

Angulo, P. (2002). Nonalcoholic fatty liver disease. N. Engl. J. Med. *346*, 1221–1231.

Araki, E., Lipes, M.A., Patti, M.E., Brüning, J.C., Haag, B., 3rd, Johnson, R.S., and Kahn, C.R. (1994). Alternative pathway of insulin signalling in mice with targeted disruption of the IRS-1 gene. Nature *372*, 186–190.

Bartz, F., Kern, L., Erz, D., Zhu, M., Gilbert, D., Meinhof, T., Wirkner, U., Erfle, H., Muckenthaler, M., Pepperkok, R., and Runz, H. (2009). Identification of cholesterol-regulating genes by targeted RNAi screening. Cell Metab. *10*, 63–75.

Basciano, H., Miller, A., Baker, C., Naples, M., and Adeli, K. (2009). LXRalpha activation perturbs hepatic insulin signaling and stimulates production of apolipoprotein B-containing lipoproteins. Am. J. Physiol. Gastrointest. Liver Physiol. *297*, G323–G332.

Berendsen, A.D., Fisher, L.W., Kilts, T.M., Owens, R.T., Robey, P.G., Gutkind, J.S., and Young, M.F. (2011). Modulation of canonical Wnt signaling by the extracellular matrix component biglycan. Proc. Natl. Acad. Sci. USA *108*, 17022–17027.

Bligh, E.G., and Dyer, W.J. (1959). A rapid method of total lipid extraction and purification. Can. J. Biochem. Physiol. *37*, 911–917.

Cheng, Z., Biechele, T., Wei, Z., Morrone, S., Moon, R.T., Wang, L., and Xu, W. (2011). Crystal structures of the extracellular domain of LRP6 and its complex with DKK1. Nat. Struct. Mol. Biol. *18*, 1204–1210.

Dalle Pezze, P., Sonntag, A.G., Thien, A., Prentzell, M.T., Gödel, M., Fischer, S., Neumann-Haefelin, E., Huber, T.B., Baumeister, R., Shanley, D.P., and Thedieck, K. (2012). A dynamic network model of mTOR signaling reveals TSC-independent mTORC2 regulation. Sci. Signal. *5*, ra25.

Darimont, C., Avanti, O., Zbinden, I., Leone-Vautravers, P., Mansourian, R., Giusti, V., and Macé, K. (2006). Liver X receptor preferentially activates de novo lipogenesis in human preadipocytes. Biochimie *88*, 309–318.

Delgado-Lista, J., Perez-Martinez, P., García-Rios, A., Phillips, C.M., Williams, C.M., Gulseth, H.L., Helal, O., Blaak, E.E., Kiec-Wilk, B., Basu, S., et al. (2011). Pleiotropic effects of TCF7L2 gene variants and its modulation in the metabolic syndrome: from the LIPGENE study. Atherosclerosis *214*, 110–116.

Du, X., Kristiana, I., Wong, J., and Brown, A.J. (2006). Involvement of Akt in ER-to-Golgi transport of SCAP/SREBP: a link between a key cell proliferative pathway and membrane synthesis. Mol. Biol. Cell *17*, 2735–2745.

Folch, J., Lees, M., and Sloane Stanley, G.H. (1957). A simple method for the isolation and purification of total lipides from animal tissues. J. Biol. Chem. *226*, 497–509.

Fujimura, N., Vacik, T., Machon, O., Vlcek, C., Scalabrin, S., Speth, M., Diep, D., Krauss, S., and Kozmik, Z. (2007). Wnt-mediated down-regulation of Sp1 target genes by a transcriptional repressor Sp5. J. Biol. Chem. *282*, 1225–1237.

Goliasch, G., Wiesbauer, F., Kastl, S.P., Katsaros, K.M., Blessberger, H., Maurer, G., Schillinger, M., Huber, K., Wojta, J., and Speidl, W.S. (2012). Premature myocardial infarction is associated with low serum levels of Wnt-1. Atherosclerosis *222*, 251–256.

Hagiwara, A., Cornu, M., Cybulski, N., Polak, P., Betz, C., Trapani, F., Terracciano, L., Heim, M.H., Rüegg, M.A., and Hall, M.N. (2012). Hepatic mTORC2 activates glycolysis and lipogenesis through Akt, glucokinase, and SREBP1c. Cell Metab. *15*, 725–738.

Hatzis, P., van der Flier, L.G., van Driel, M.A., Guryev, V., Nielsen, F., Denissov, S., Nijman, I.J., Koster, J., Santo, E.E., Welboren, W., et al. (2008). Genome-wide pattern of TCF7L2/TCF4 chromatin occupancy in colorectal cancer cells. Mol. Cell. Biol. *28*, 2732–2744.

Hua, X., Nohturfft, A., Goldstein, J.L., and Brown, M.S. (1996). Sterol resistance in CHO cells traced to point mutation in SREBP cleavage-activating protein. Cell *87*, 415–426.

Huertas-Vazquez, A., Plaisier, C., Weissglas-Volkov, D., Sinsheimer, J., Canizales-Quinteros, S., Cruz-Bautista, I., Nikkola, E., Herrera-Hernandez, M., Davila-Cervantes, A., Tusie-Luna, T., et al. (2008). TCF7L2 is associated with high serum triacylglycerol and differentially expressed in adipose tissue in families with familial combined hyperlipidaemia. Diabetologia *51*, 62–69.

Kaytor, E.N., Zhu, J.L., Pao, C.I., and Phillips, L.S. (2001). Physiological concentrations of insulin promote binding of nuclear proteins to the insulin-like growth factor I gene. Endocrinology *142*, 1041–1049.

Krieg, R.C., Liotta, L.A., Petricoin, E.F., 3rd, and Herrmann, P.C. (2004). Trapping radioactive carbon dioxide during cellular metabolic assays under standard culture conditions: description of a unique gas-capturing device. J. Biochem. Biophys. Methods *58*, 119–124.

Laplante, M., and Sabatini, D.M. (2009). An emerging role of mTOR in lipid biosynthesis. Curr. Biol. *19*, R1046–R1052.

Li, T., Chen, Y.H., Liu, T.J., Jia, J., Hampson, S., Shan, Y.X., Kibler, D., and Wang, P.H. (2003). Using DNA microarray to identify Sp1 as a transcriptional regulatory element of insulin-like growth factor 1 in cardiac muscle cells. Circ. Res. *93*, 1202–1209.

Liu, W., Mani, S., Davis, N.R., Sarrafzadegan, N., Kavathas, P.B., and Mani, A. (2008). Mutation in EGFP domain of LDL receptor-related protein 6 impairs cellular LDL clearance. Circ. Res. *103*, 1280–1288.

Mani, A., Radhakrishnan, J., Wang, H., Mani, A., Mani, M.A., Nelson-Williams, C., Carew, K.S., Mane, S., Najmabadi, H., Wu, D., and Lifton, R.P. (2007). LRP6 mutation in a family with early coronary disease and metabolic risk factors. Science *315*, 1278–1282.

Morrison, W.R., and Smith, L.M. (1964). Preparation of fatty acid methyl esters and dimethylacetals from lipids with boron fluoride methanol. J. Lipid Res. *5*, 600–608.

Perez-Martinez, P., Perez-Caballero, A.I., Garcia-Rios, A., Yubero-Serrano, E.M., Camargo, A., Gomez-Luna, M.J., Marin, C., Gomez-Luna, P., Dembinska-Kiec, A., Rodriguez-Cantalejo, F., et al. (2012). Effects of rs7903146 variation in the Tcf7l2 gene in the lipid metabolism of three different populations. PLoS ONE *7*, e43390.

Singh, R., De Aguiar, R.B., Naik, S., Mani, S., Ostadsharif, K., Wencker, D., Sotoudeh, M., Malekzadeh, R., Sherwin, R.S., and Mani, A. (2013a). LRP6 enhances glucose metabolism by promoting TCF7L2-dependent insulin receptor expression and IGF receptor stabilization in humans. Cell Metab. *17*, 197–209.

Singh, R., Smith, E., Fathzadeh, M., Liu, W., Go, G.W., Subrahmanyan, L., Faramarzi, S., McKenna, W., and Mani, A. (2013b). Rare nonconservative LRP6 mutations are associated with metabolic syndrome. Hum. Mutat. *34*, 1221–1225.

Tomaszewski, M., Charchar, F.J., Barnes, T., Gawron-Kiszka, M., Sedkowska, A., Podolecka, E., Kowalczyk, J., Rathbone, W., Kalarus, Z., Grzeszczak, W., et al. (2009). A common variant in low-density lipoprotein receptor-related protein 6 gene (LRP6) is associated with LDL-cholesterol. Arterioscler. Thromb. Vasc. Biol. *29*, 1316–1321.

Wang, Y., Kurdi-Haidar, B., and Oram, J.F. (2004). LXR-mediated activation of macrophage stearoyl-CoA desaturase generates unsaturated fatty acids that destabilize ABCA1. J. Lipid Res. *45*, 972–980.

Yabe, D., Brown, M.S., and Goldstein, J.L. (2002). Insig-2, a second endoplasmic reticulum protein that binds SCAP and blocks export of sterol regulatory element-binding proteins. Proc. Natl. Acad. Sci. USA *99*, 12753–12758.

Yang, T., Espenshade, P.J., Wright, M.E., Yabe, D., Gong, Y., Aebersold, R., Goldstein, J.L., and Brown, M.S. (2002). Crucial step in cholesterol homeostasis: sterols promote binding of SCAP to INSIG-1, a membrane protein that facilitates retention of SREBPs in ER. Cell *110*, 489–500.

Ye, Z.J., Go, G.W., Singh, R., Liu, W., Keramati, A.R., and Mani, A. (2012). LRP6 protein regulates low density lipoprotein (LDL) receptor-mediated LDL uptake. J. Biol. Chem. *287*, 1335–1344.

Yecies, J.L., Zhang, H.H., Menon, S., Liu, S., Yecies, D., Lipovsky, A.I., Gorgun, C., Kwiatkowski, D.J., Hotamisligil, G.S., Lee, C.H., and Manning, B.D. (2011). Akt stimulates hepatic SREBP1c and lipogenesis through parallel mTORC1-dependent and independent pathways. Cell Metab. *14*, 21–32.

Yuan, M., Pino, E., Wu, L., Kacergis, M., and Soukas, A.A. (2012). Identification of Akt-independent regulation of hepatic lipogenesis by mammalian target of rapamycin (mTOR) complex 2. J. Biol. Chem. *287*, 29579–29588.

Zhu, J.L., Kaytor, E.N., Pao, C.I., Meng, X.P., and Phillips, L.S. (2000). Involvement of Sp1 in the transcriptional regulation of the rat insulin-like growth factor-1 gene. Mol. Cell. Endocrinol. *164*, 205–218.